Research Article

Wenwen Xu, Shanguang Zhao, Liang Li, Lele Fan, Jian Yuan, Yumeng Zhang, Bing Li, Zhongliang Liu*, and Qinzhuang Liu*

Preparation of VO_2/graphene/SiC film by water vapor oxidation

https://doi.org/10.1515/rams-2023-0338
received February 11, 2023; accepted June 14, 2023

Abstract: Vanadium dioxide (VO_2) has attracted extensive attention due to the specific metal-insulator phase transition as well as the wide device applications. The practical performance of VO_2-based device strongly depends on the quality of VO_2, since the higher quality of VO_2 film always shows much more pronounced phase transition behavior. Thus, the preparation of high quality VO_2 film is essential and highly desirable. In this work, we have prepared high-quality VO_2 film on SiC substrate by water vapor oxidation with graphene (G) buffer layer, which showed excellent phase transformation properties. Compared with the VO_2/SiC sample without G buffer layer, the VO_2/G/SiC films show the resistance changes up to four-orders of magnitude across the phase transition boundary and superior optoelectronic properties, which indicates the significant role of G layer in the film growth process. The current study not only provides an economical and feasible method for VO_2/G/SiC thin film preparation with high quality, but also supply some clues for the application of G-based VO_2 devices in the future.

Keywords: water vapor oxidation, vanadium dioxide films, phase transformation properties, X-ray diffraction, molecular beam epitaxy

*** Corresponding author: Zhongliang Liu,** School of Physics and Electronic Information, Huaibei Normal University, Huaibei 235000, China, e-mail: zlliu@chnu.edu.cn
*** Corresponding author: Qinzhuang Liu,** School of Physics and Electronic Information, Huaibei Normal University, Huaibei 235000, China, e-mail: qzliu@mail.ustc.edu.cn
Wenwen Xu, Jian Yuan, Yumeng Zhang, Bing Li: School of Physics and Electronic Information, Huaibei Normal University, Huaibei 235000, China
Shanguang Zhao: School of Nuclear Science and Technology, University of Science and Technology of China, Hefei, Anhui 230029, China; National Synchrotron Radiation Laboratory, University of Science and Technology of China, Hefei 230029, China
Liang Li: School of Nuclear Science and Technology, University of Science and Technology of China, Hefei, Anhui 230029, China
Lele Fan: Key Laboratory for Advanced Technology in Environmental Protection of Jiangsu Province, Yancheng Institute of Technology, Yancheng 224051, China

1 Introduction

As a typical correlated oxide material, Vanadium dioxide (VO_2) has attracted great interest because of the metal-insulator phase transition (MIT) near 68°C [1–3]. This specific MIT behavior of VO_2 always showed sharp resistivity change with the 4–5 orders of magnitude and pronounced optical switching effects, which made it promising for a wide range of applications in optical switching devices [4,5], smart windows [6,7], memory devices [8,9], infrared laser protection [10], supercapacitor [11] and lithium storage device [12].

It was known that the practical performance of VO_2 based device strongly depends on the quality of VO_2, since the excellent single crystal VO_2 film always showed pronounced phase transition behavior. Thus, the preparation of high quality VO_2 film is essential and highly desirable. Currently, various VO_2 film preparation techniques have been developed, including the pulsed laser deposition [13,14], molecular beam epitaxy (MBE) [15,16], magnetron sputtering and other physical deposition technologies. However, these methods often required complex parameter control processes and expensive equipment, which seriously limited their practical applications. Direct thermal oxidation of V film in oxygen atmosphere was a much simpler method. However, due to the polyvalent properties of V atoms, the oxidation of V film was not easy to be controlled for pure VO_2 film preparation [17,18]. Thus, during the traditional oxidation process of V film, the film was sensitive to the gas pressure and annealing parameters, which greatly affected the pure VO_2 film preparation with high quality. Different from the usual thermal oxidation, the wet oxidation technology was considered as a relatively mild oxidation method, which was able to avoid the peroxidation of the VO_2 film [19–21]. The water oxidation

device was simple and easy to operate, which was suitable for the preparation of high-quality films on large substrates, which lay a foundation for the practical application of the device. More importantly, it was easy to prepare high-quality VO_2 film with large size, which was beneficial for the practical applications.

The growth of high-quality VO_2 thin film also needed to consider the lattice match between the film and substrate. In fact, the substrate with lattice matching and photoelectric characteristics played an active role in the preparation of high quality VO_2 films as well as the practical application of the devices. It was known that graphene (G) layer had attracted a lot of attention because of unique properties. Normally, the G single layer was a semi-metal with Dirac fermions (zero effective mass) as charge carriers, which could produce extraordinary effects, such as mobility up to 200,000 $cm^2 \cdot V^{-1} \cdot S^{-1}$ [22], ballistic distances up to one micron at room temperature. If a phase transition VO_2 film is combined with G layer, some interesting optical and electrical properties would be integrated for some functional device applications. In fact, the fast adaptive thermal camouflage based on flexible VO_2/G/CNT films had been successfully fabricated [23]. The enhanced optical response of VO_2 doped into G films was also observed [24]. In addition, VO_2 film deposited on G/Ge substrate or SiC substrate was studied to examine the phase transition behavior [25]. However, using G as the buffer layer to prepare high-quality VO_2 film on SiC crystal substrate had not been reported.

In this work, homogeneous and pure monoclinic VO_2/G/SiC film with excellent MIT performance were prepared by wet oxidation method. The effects of annealing time and Ar flux rate on the properties of VO_2 films were systematically investigated. The results showed that the continuous VO_2/G/SiC film exhibited resistance changes of nearly four-orders of magnitude. As a mild oxidation method, the current wet oxidation technique inhibited the peroxidation process of V, thus pure VO_2 film was obtained. In addition, by using the G as a buffer layer, the quality of the VO_2 film was further improved, which showed more pronounced phase transformation properties.

2 Experiment

Single crystal silicon carbide (0001) (6H–SiC) was cleaned by RCA process [26]. The vacuum of the MBE device was kept at 1×10^{-7} Pa. The SiC substrate was first heated to 300°C to eliminate impurities such as water vapor. At the substrate temperature of 300°C, Cu atoms were deposited on SiC substrate in the MBE chamber and the deposition time was 10 min. Then, the samples were annealed at 1,380°C for different times. With the assistance of Cu atoms, the G layers were successfully prepared on SiC substrate.

The V element was deposited on G surface at room temperature by sputtering for 30 min in the magnetron sputtering equipment and the deposition rate was about 7 $nms \cdot min^{-1}$. The V/G/SiC samples were put into the water oxidation system, and the appropriate amount of argon (Ar) gas was introduced to oxidize the prepared metal film at 550°C. Ar as carrier gas was controlled by a mass flow controller and bubbles were generated after piped into the water bath bottle. The flask was placed in a water bath, which was heated to produce steam. The water bath temperature and Ar flow controlled the water vapor content in the furnace. In the water oxidation system, a certain amount of argon was introduced to oxidize the prepared metal films. During the wet oxidation, the water flask half-filled with deionized water was kept in the water bath at a temperature of 79°C. The detailed schematics are described in Figure 1 [27].

The samples were tested by Raman spectrometer (λ = 532 nm), and the surface morphologies were examined by field emission electron microscopy (SU8220, Hitachi, Japan). X-ray photoelectron spectroscopy (XPS, AXIS SUPRA$^+$, Al Kα) was used to analyze the chemical state of the samples. High-resolution X-ray Diffractometer (XRD, Panalytical, the Netherlands) was used to test the crystal structure. Step size and time per step of the XRD measurements were 0.005° and 0.3 s, accordingly. The working voltage of the XRD equipment is 40 kV and the working current is 40 mA. In addition, the phase

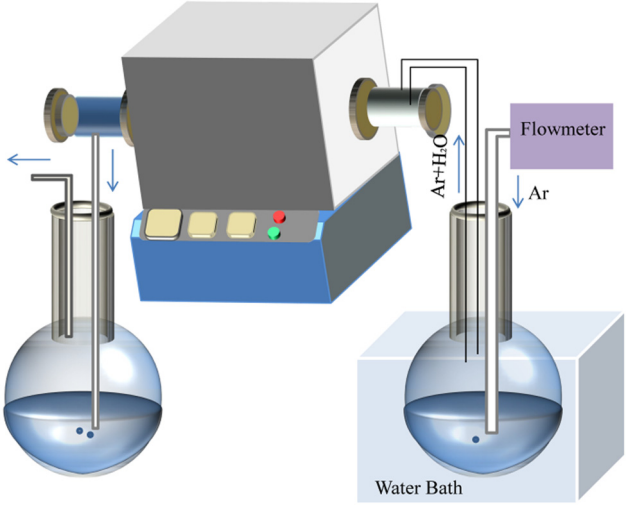

Figure 1: Schematic diagram of water vapor assisted oxidation. The tube furnace and flow meter recorded the temperature and flow of Ar gas, Ar and water vapor entered the tube furnace and oxidized V metal film.

transition performance of the samples was characterized by using a home-made four-probe test system with a variable temperature sample stage.

3 Results

The quality of G greatly affected the crystallinity of VO_2. Under the assistance of Cu atoms pre-deposition, the G layers were obtained on the top surface of SiC single crystal substrate. The characterized spectra and schematic illustration diagram of the G sample are shown in Figure 2. From Figures 2(a), D, G and 2D peaks at 1,360, 1,590 [28] and 2,730 cm^{-1} [29,30] can be observed, respectively. The strong G and 2D peaks proved the existence of high-quality G. The weak D peaks indicated that the G on the SiC surface had fewer defects and better crystal quality. Moreover, the absence of other peaks also implied that only G existed on the surface of SiC. The grain size (La) of G was calculated using the following formula [31]:

$$\mathrm{La(nm)} = \frac{560}{E_l^4}\left(\frac{I_D}{I_G}\right). \quad (1)$$

Thus, the grain size of G was estimated to be about 73 nm.

Figure 2(b) showed the XPS spectrum of the G/SiC sample. The characteristic peak of the samples were divided into G with binding energy of 284.4 eV, surface buffer layer of 284.9 eV and SiC substrate of 283.3 eV, respectively [32,33]. The peak centered at 284.4 eV was related to sp^2 hybridization in the G layer. The asymmetry of the C 1s peak in the direction of higher binding energies was a sign of defects in sp^3 hybridized orbital carbon atoms, with a broad peak at 284.9 eV [34,35]. The dominant G content suggested that the samples underwent an adequate annealing process, and high-quality G was prepared on the surface of silicon carbide, which was consistent with Raman measurements.

In order to investigate the surface morphology of G, the G/SiC sample was characterized by SEM. It was observed that the G film was continuous and uniformly distributed over large areas with very few surface defects in Figure 2(c).

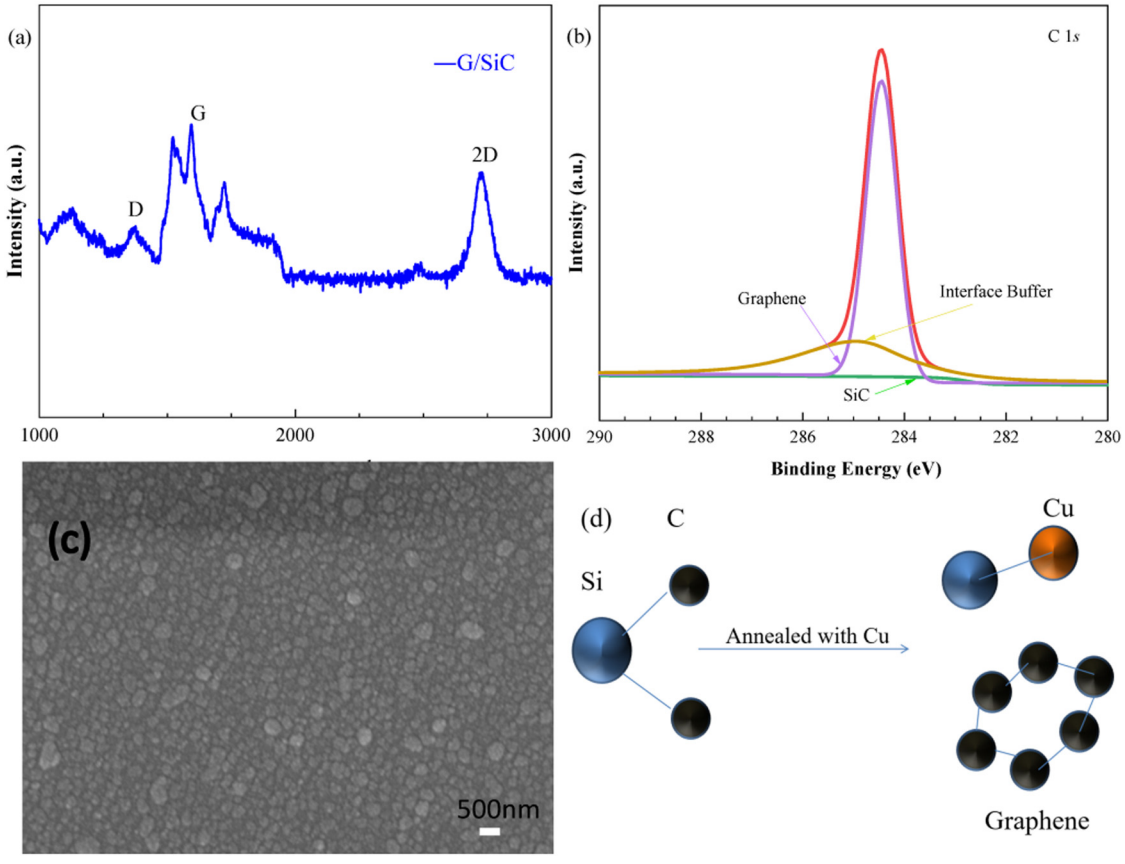

Figure 2: (a) Raman spectra of the samples prepared by annealing of SiC after introduction of Cu atoms, (b) the XPS spectra C 1s of the G/SiC samples, (c) surface morphology of the G/SiC as examined by SEM, and (d) schematic illustration of the reaction happened during the deposition. The black, blue and brown spheres represented C, Si and Cu atoms, respectively. Reaction equation: SiC + Cu → copper silicide + C (G).

The binding process of copper and silicon atoms promoted the reconstruction of carbon atoms on the surface of SiC, which improved the crystallinity of G. The schematic diagram of G/SiC sample preparation is shown in Figure 2(d). Compared with traditional annealing treatment for SiC single crystal for G preparation, the introduced Cu atoms on SiC surface would lead to higher quality G layer formation. This is contrary to the fact that the SiC and Cu were combined to form copper silicide, and carbon atoms were reconstructed on the surface of SiC [36].

It was suggested that after the Cu atoms were deposited on SiC surface, the annealing time was a key factor for G layer formation by the annealing treatment at 1,380°C. In addition, the quality of the formed G layer further affected the VO_2 film growth. Thus, by controlling the annealing time of Cu/SiC, a series of G/SiC were obtained. And then, metallic V layer was deposited onto these G/SiC substrate. By using the wet oxidation method, VO_2/G/SiC films were finally prepared and analyzed by XRD tests. Figure 3(a) shows the XRD pattern of VO_2/G/SiC samples with different annealing times. When the annealing time was 10 min, there was no characteristic peak. However, when the annealing time reached 60 min, the sample had a strong characteristic peak at 2θ = 39.89°, indicating that the preferred orientation of the sample was (020) plane (JCPDS card #82-0661) [5,37,38]. The resistance measurements as the function of temperature (R–T curve) for the VO_2/G/SiC samples are shown in Figure 3(b). It was clear that the phase transition curve of the samples with annealing time of 10 and 90 min were relatively smooth, which showed the resistance change of only one. However, the sample with the annealing time of 60 min showed the resistance change of 3–4 orders of magnitude during the phase transition process. These results were in good agreement with the XRD measurement, which indicated that the annealing treatment with 60 min was more suitable for the VO_2/G/SiC sample preparation. In this case, the G layer played a great role in promoting the property of VO_2 film. Meanwhile, the results showed that the water oxidation technology could be used to prepare VO_2 film with excellent electrical properties on the G/SiC substrate.

The Ar flux also affected the water vapor oxidation effect and regulated the quality of VO_2. Figure 4(a) shows the Raman spectra of the VO_2/G/SiC samples at different Ar flux rates. All samples showed peaks of different intensities at 138, 193, 224, 258, 307, 337, 387, 440, 497 and 612 cm^{-1}, which were quite consistent with the characteristic peaks of monoclinic VO_2(M-VO_2) [39–41]. The crystal structures were characterized by XRD with the θ–2θ scan mode and the results were demonstrated in Figure 4(b). It was observed that the unique peak around 2θ = 39.9° was assigned to the diffraction from monoclinic VO_2 (020) (JCPDS card #82-0661). This indicated that 0.6 $L{\cdot}min^{-1}$ was the best Ar flow condition for the preparation of VO_2/G/SiC sample. It was worth noting that all samples had strong characteristic peaks at 2θ = 37°, which was speculated to generate other vanadium oxides.

The chemical state of the obtained VO_2/G/SiC film with the Ar flow rate of 0.6 $L{\cdot}min^{-1}$ were examined by XPS in Figure 4(c). The detailed XPS curve-fittings are shown in Figure 4(d) and (e). The O 1s peak at 530 eV mainly originated from the O–V bond and the O 1s peak at 531.5 eV should be attributed to the –OH adsorbed on the surface. Similarly, V $2p_{3/2}$ had a peak binding energy of 516.1 eV and 517.3 eV [42]. The appearance of V^{4+} peak at 516 eV

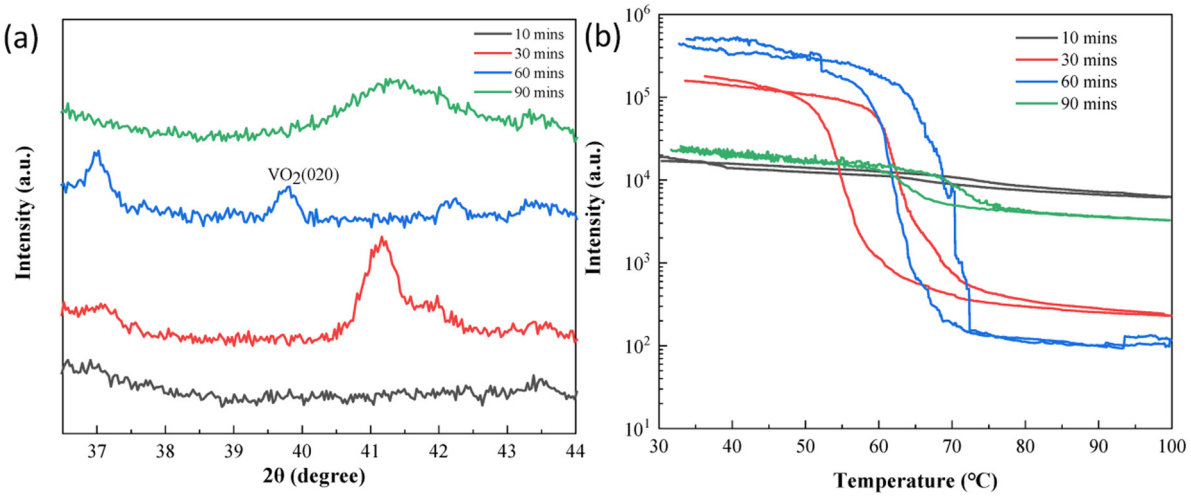

Figure 3: (a) The XRD pattern of the different annealing times of Cu/SiC substrate, (b) R–T curve measurements for the prepared VO_2/G/SiC film by water vapor assisted oxidation at different annealing times.

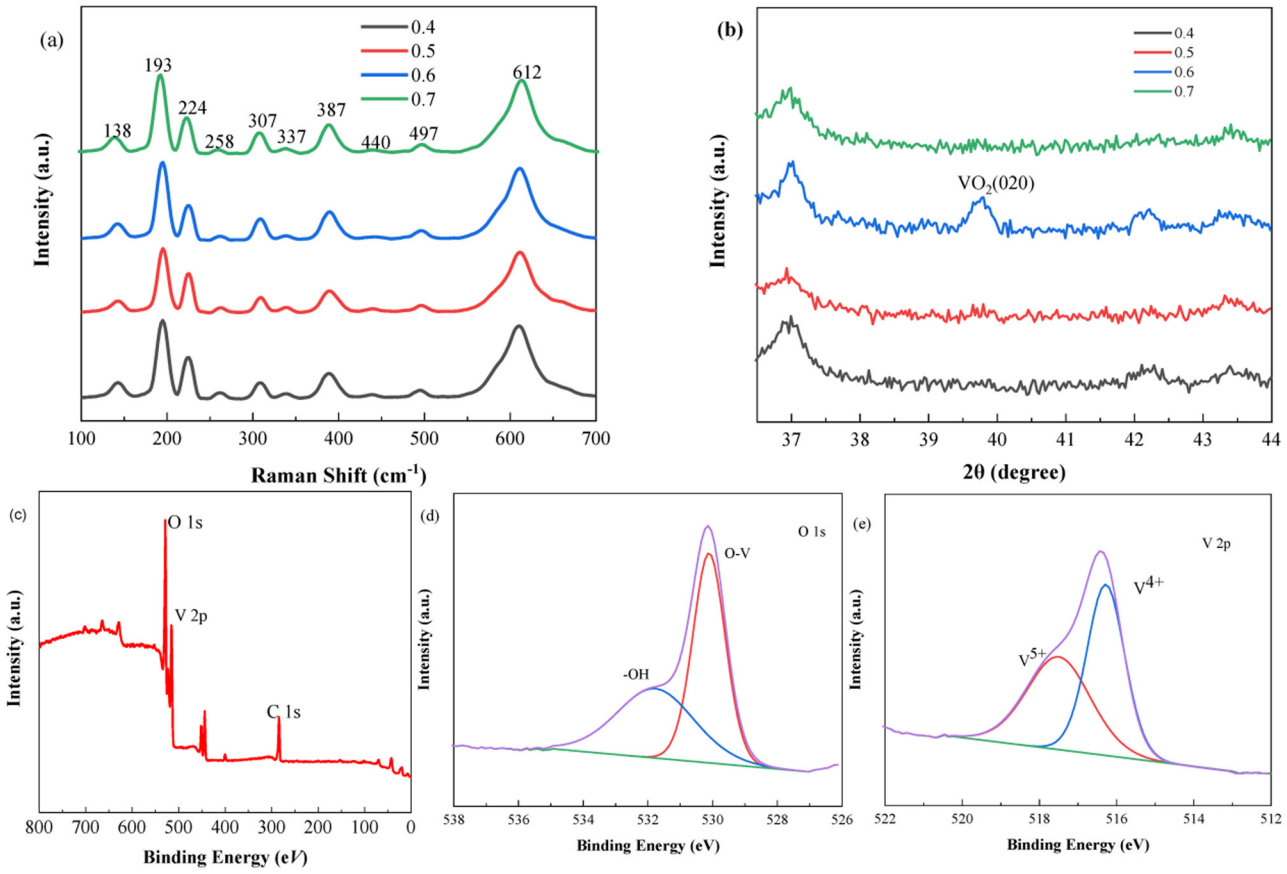

Figure 4: (a) Raman spectrum, (b) XRD pattern of the prepared VO_2/G/SiC samples at different Ar flow (unit: L·min^{-1}), (c) XPS spectrum, (d) and (e) show the curve-fittings of O 1s and V 2p peaks for the VO_2/G/SiC films at Ar flow rate of 0.6 L·min^{-1} by water vapor assisted oxidation.

indicated the formation of VO_2 on the substrate surface [43], while the presence of a higher binding energy of 517.3 eV indicated that the sample contained a small amount of V^{5+} This may be due to a slight surface oxidation of the sample when exposed to air. From the above characterizations, it was clear that the obtained VO_2/G/SiC film produced by water vapor oxidation at the Ar flow rate of 0.6 L·min^{-1} showed the pure monoclinic phase structure and excellent stoichiometry.

The surface morphology of the samples was characterized by SEM and is shown in Figure 5(a–d). When the Ar flow rate was 0.4 L·min^{-1}, the grain size of the sample surface was small and the particle size was varied. When the Ar flow rate increased to 0.5 L·min^{-1}, the surface particles were randomly distributed in island shape and the film continuity was discontinuous and a few holes appeared. When the Ar flow rate increased to 0.6 L·min^{-1}, the continuity of the sample was improved and no holes existed. For the sample fabrication at the Ar flow rate of 0.7 L·min^{-1}, the grain size started to decrease again. The experimental results demonstrated that the optimal argon oxide flow of the VO_2/G/6H–SiC film was 0.6 L·min^{-1}, which was consistent with the results obtained by XPS and Raman tests. Figure 5(e) shows a cross-section image of the sample and the distribution of each element. The cross-section image mainly contains three colors corresponding to the three-layer structure of the sample. This diagram served as proof of the existence of the VO_2/G/6H–SiC film.

In order to further study the electrical properties of the samples, a four-probe variable temperature resistance tester was used to measure the resistance–temperature curves (*R–T*) of the films. Figure 6(a) shows the *R–T* curves of the VO_2/G/SiC films at different Ar flow rates. When the Ar flow rate was 0.4, 0.5 and 0.7 L·min^{-1}, the resistivity changes were only two- or three-orders of magnitude. For the sample fabricated at the argon flow rate of 0.6 L·min^{-1}, the resistivity changes were nearly four-orders of magnitude. When the argon flow rate increased from 0.4 to 0.6 L·min^{-1}, the *R–T* curve became sharper and the resistance ratio between the insulating metal phases increased during the MIT process. Accordingly, the change in *R–T* curve further determined that 0.6 L·min^{-1} should be the optimal argon flow

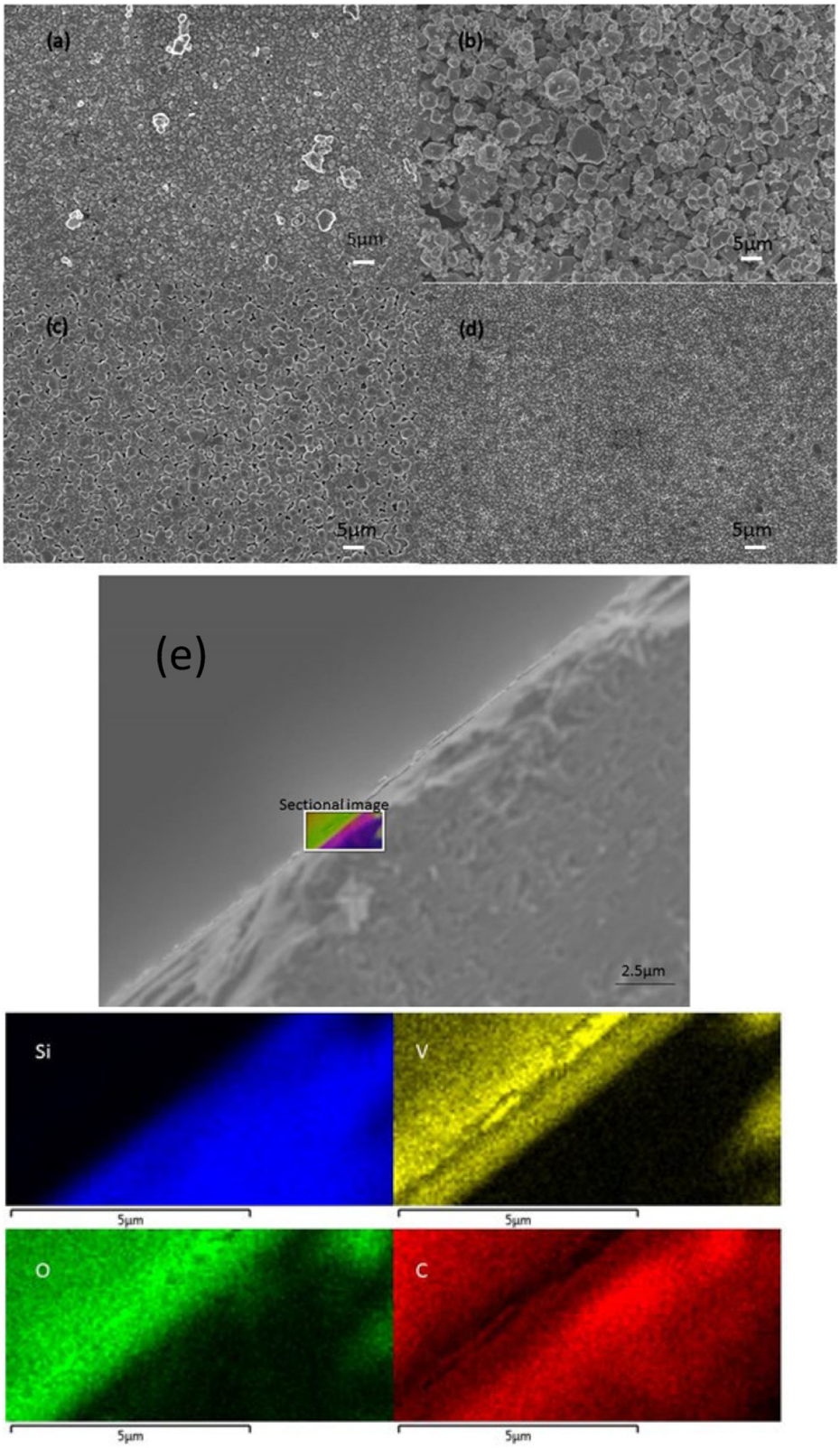

Figure 5: (a)–(d) SEM images of the VO_2/G/SiC film prepared by wet oxidation at a flow rate of 0.4, 0.5, 0.6 and 0.7 L·min^{-1}, respectively. (e) The sectional image of the VO_2/G/SiC film fabricated by water vapor assisted method at a flow rate of 0.6 L·min^{-1}.

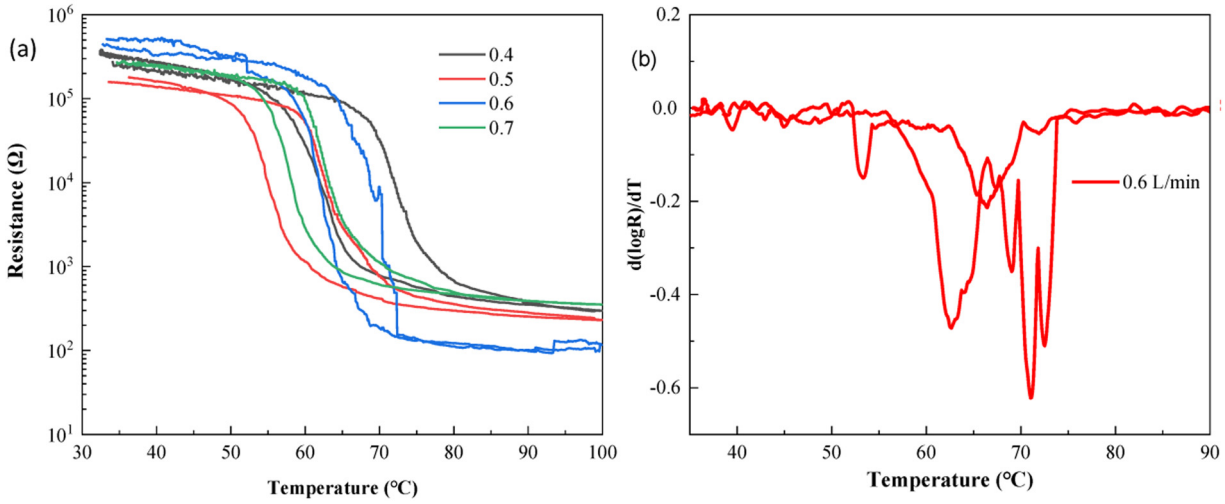

Figure 6: (a) The *R*–*T* curve for the VO_2/G/SiC film prepared by wet oxidation at different Ar flow rates (unit: L·min^{-1}) and (b) related differential curves for the optimized VO_2/G/SiC film at a flow rate of 0.6 L·min^{-1}.

for wet oxidation. The results showed that VO_2 film prepared by wet oxidation had good electrical properties, and the resistance variation reached nearly four-orders of magnitude after optimization. As a buffer layer, high-quality G had excellent optical and electrical properties, which further improved the electrical properties of VO_2 and also extended the application range of devices. The related differential curve for the optimized VO_2/G/SiC film at the flow rate of 0.6 L·min^{-1} is shown in Figure 5(b). Critical transition temperatures (T_{heat} and T_{cool}) are defined as the corresponding peak positions of the Gaussian fitted $d(\log(R))/dT$ curve during heating and cooling, respectively. Phase transition temperature is defined as $T_{MIT} = (T_{heat} + T_{cool})/2$. The critical temperatures were determined as 62.0°C for the cooling process and 70.8°C for the heating process, which were quite consistent with the previous reports by other deposition techniques [19,44,45]. The thermally induced width ($T_{heat} - T_{cool}$) of the sample was 8.8°C and the phase transition temperature was 66.4°C.

To investigate the effect of G on the preparation of VO_2, the *R*–*T* curves of VO_2/6H–SiC and VO_2/G/6H–SiC films are shown in Figure 7. It can be seen that under the same experimental conditions, the resistivity change of VO_2/G/SiC film was close to four-orders of magnitude and the phase transition temperature was closer to that of VO_2 [46–50], while the resistivity change of VO_2/SiC film was

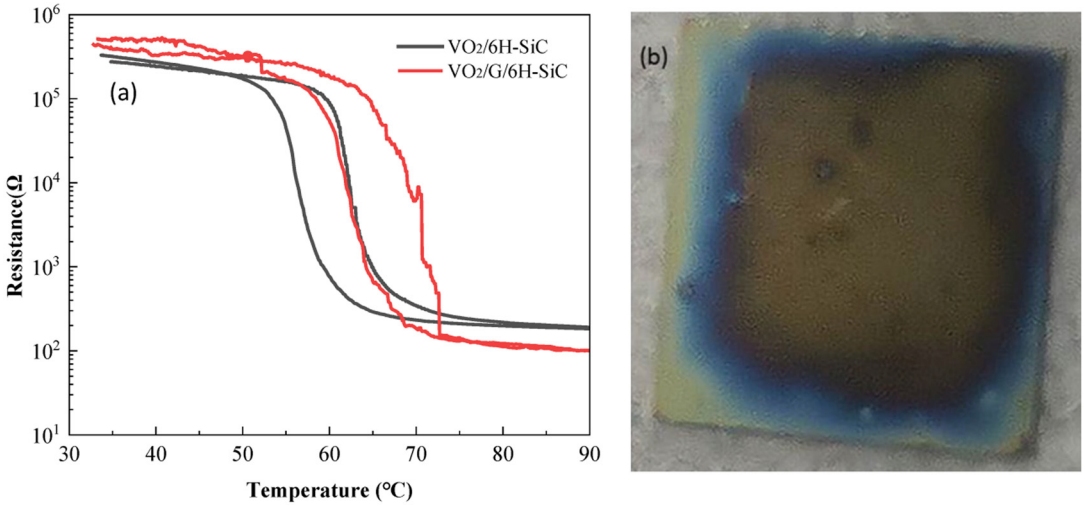

Figure 7: (a) After optimization, *R*–*T* results of VO_2/G/SiC and VO_2/SiC thin films under the same experimental conditions and (b) the optical photo of the sample obtained under optimal synthesis conditions (the annealing time of SiC was 60 min and the Ar gas flow rate was 0.6 L·min^{-1}).

only close to three-orders of magnitude. This indicated that doped G increased the resistivity of VO_2/SiC film and improved the quality of VO_2 after optimization. The optical photo of the sample obtained under optimal synthesis conditions (60 min, 0.6 L·min^{-1}) is shown in Figure 7(b). Although the film has not been prepared on large-size substrate in this study, some research groups have prepared high-quality VO_2 on large-size Si wafers by wet oxidation method, indicating that the film can be prepared on large-size substrate by this method. Based on this fact, our group attempted to prepare VO_2 films on G/SiC substrate, which paved the way for large size SiC substrate related applications.

4 Conclusion

In conclusion, high quality VO_2/G/SiC films were successfully prepared by moderate water oxidation technique. The experimental results showed that the G-based VO_2 films with resistance variation of nearly four-orders of magnitude exhibited excellent electrical properties and crystallinity. In the water oxidation method, water vapor as a moderate oxidant was used to effectively oxidize the metal V precursor film into a pure M–VO_2 film. Graphene, as a buffer layer, had excellent photoelectric properties, which further improved the electrical properties of VO_2 and broadened the application range of related devices. This work provided a facile and modest method for the preparation of VO_2 films, which was of practical significance for the further application of G-based VO_2 devices in the future.

Funding information: This work was partially supported by Natural Science Foundation of China (51402120 and 11974127), Natural Science Foundation of Anhui Higher Education Institutions of China (KJ2019ZD40) and Anhui Natural Science Foundation (2108085QA30).

Author contributions: All authors have accepted responsibility for the entire content of this manuscript and approved its submission.

Conflict of interest: The authors state no conflict of interest.

References

[1] Fan, L. L., S. Chen, G. M. Liao, Y. L. Chen, H. Ren, and C. W. Zou. Comprehensive studies of interfacial strain and oxygen vacancy on metal-insulator transition of VO_2 film. *Journal of Physics: Condensed Matter*, Vol. 28, 2016, id. 255002.

[2] Théry, V., A. Boulle, A. Crunteanu, J. C. Orlianges, A. Beaumont, R. Mayet, et al. Structural and electrical properties of large area epitaxial VO_2 films grown by electron beam evaporation. *Journal of Applied Physics Letters*, Vol. 121, 2017, id. 055303.

[3] Zhang, H. T., L. Zhang, D. Mukherjee, Y. X. Zheng, R. C. Haislmaier, N. Alem, et al. Wafer-scale growth of VO_2 thin films using a combinatorial approach. *Nat Comm*, Vol. 6, 2015, id. 8475.

[4] Liu, K., D. Y. Fu, J. B. Cao, J. Suh, K. X. Wang, C. Cheng, et al. Dense electron system from gate-controlled surface metal-insulator transition. *Nano Letters*, Vol. 12, 2012, pp. 6272–6277.

[5] Chen, F. H., L. L. Fan, S. Chen, G. M. Liao, Y. L. Chen, P. Wu, et al. Control of the metal-insulator transition in VO_2 epitaxial film by modifying carrier density. *ACS Applied Materials & Interfaces*, Vol. 7, 2015, pp. 6875–6881.

[6] Hao, Q., W. Li, H. Y. Xu, J. W. Wang, Y. Yin, H. Y. Wang, et al. VO_2/TiN Plasmonic thermochromic smart coatings for room-temperature applications. *Advanced Materials*, Vol. 30, 2018, id. 1705421.

[7] Chang, T. C., X. Cao, N. Li, S. W. Long, X. Gao, L. R. Dedon, et al. Facile and low-temperature fabrication of thermochromic Cr_2O_3/VO_2 smart coatings: enhanced solar modulation ability, high luminous transmittance and UV-shielding function. *ACS Applied Materials & Interfaces*, Vol. 9, 2017, pp. 26029–26037.

[8] Xue, W. H., G. Liu, Z. C. Zhong, Y. H. Dai, J. Shang, Y. W. Liu, et al. A 1D vanadium dioxide nanochannel constructed via electric-field-induced ion transport and its superior metal-insulator transition. *Advanced Materials*, Vol. 29, 2017, id. 1702162.

[9] Javier, D. V., S. Pavel, T. Federico, N. M. Vargas, Y. Kalcheim, P. Wang, et al. Subthreshold firing in Mott nanodevices. *Nature*, Vol. 569, 2019, pp. 388–392.

[10] Fan, L. L., Y. L. Chen, Q. H. Liu, S. Chen, L. Zhu, Q. Q. Meng, et al. Infrared response and optoelectronic memory device fabrication based on epitaxial VO_2 film. *ACS Applied Materials & Interfaces*, Vol. 8, 2016, pp. 32971–32977.

[11] Lv, W. F., C. Yang, G. Meng, R. F. Zhao, A. J. Han, R. Wang, et al. VO_2(B) nanobelts/reduced graphene oxide composites for high-performance flexible all-solid-state supercapacitors. *Scientific Reports*, Vol. 9, 2019, id. 10831.

[12] Li, S., Y. Cen, Q. Xiang, K. A. Muhammad, B. B. Hu, W. Li, et al. Vanadium dioxide-reduced graphene oxide binary host as an efficient polysulfide plague for high-performance lithium–sulfur batteries. *Journal of Materials Chemistry A*, Vol. 7, 2019, pp. 1658–1668.

[13] Fan, L. L., Y. F. Wu, C. Si, C. W. Zou, Z. M. Qi, L. B. Li, et al. Oxygen pressure dependent VO_2 crystal film preparation and the interfacial epitaxial growth study. *Thin Solid Films*, Vol. 520, 2012, pp. 6124–6129.

[14] Alok, G., N. Jagdish, and D. Titas. Near bulk semiconductor to metal transition in epitaxial VO_2 thin films. *Applied Physics Letters*, Vol. 97, 2010, id. 151912.

[15] Fan, L. L., S. Chen, Y. F. Wu, F. H. Chen, W. S. Chu, X. Chen, et al. Growth and phase transition characteristics of pure M-phase VO_2 epitaxial film prepared by oxide molecular beam epitaxy. *Applied Physics Letters*, Vol. 103, 2013, id. 131914.

[16] Lee, S., T. L. Meyer, P. Sungkyun, E. Takeshi, and H. N. Lee. Growth control of the oxidation state in vanadium oxide thin films. *Applied Physics Letters*, Vol. 105, 2014, id. 223515.

[17] Ferran, U. B., C. Aurelian, and J. P. Raskin. Raman and XPS characterization of vanadium oxide thin films with temperature. *Applied Surface Science*, Vol. 403, 2017, pp. 717–727.

[18] Geert, R., B. D. Schutter, D. Wouter, M. Koen, R. Iuliana, and D. Christophe. In situ X-ray diffraction study of the controlled oxidation and reduction in the V–O system for the synthesis of VO_2 and V_2O_3 thin films. *Journal of Material Chemistry C*, Vol. 3, 2015, pp. 11357–11365.

[19] Liang, W. Z., M. Gao, C. Lu, Z. Zhang, C. H. Chan, L. J. Zhuge, et al. Enhanced metal-insulator transition performance in scalable vanadium dioxide thin films prepared using a moisture-assisted chemical solution approach. *ACS Applied Materials & Interfaces.*, Vol. 10, 2018, pp. 8341–8348.

[20] Luo, L. L., M. Su, P. F. Yan, L. F. Zou, D. K. Schreiber, D. R. Baer, et al. Atomic origins of water-vapour-promoted alloy oxidation. *Nature Mater*, Vol. 17, 2018, pp. 514–518.

[21] Chen, R. Q., C. W. Zou, X. D. Yan, A. Ahmed, and W. Gao. Growth mechanism of ZnO nanostructures in wet-oxidation process. *Thin Solid Films*, Vol. 519, 2011, pp. 1837–1844.

[22] Chen, J. H., C. Jang, S. Xiao, M. Ishigami, and M. S. Fuhrer. Intrinsic and extrinsic performance limits of graphene devices on SiO_2. *National Nanotechnology*, Vol. 3, 2008, pp. 206–209.

[23] Xiao, L., H. Ma, J. K. Liu, W. Zhao, Y. Jia, Q. Zhao, et al. Fast adaptive thermal camouflage based on flexible VO_2/graphene/CNT thin films. *Nano Letters*, Vol. 15, 2015, pp. 8365–8370.

[24] Kim, H., Y. Kim, T. Y. Kim, A. R. Jang, Y. J. Hu, H. H. Seung, et al. Enhanced optical response of hybridized VO_2/graphene films. *Nanoscale*, Vol. 5, 2013, pp. 2632–2636.

[25] Zhou, H. J., J. H. Li, Y. C. Xin, X. Cao, S. H. Bao, and P. Jin. Electron transfer induced thermochromism in a VO_2–graphene–Ge heterostructure. *Journal of Material Chemistry C*, Vol. 3, 2015, pp. 5089–5097.

[26] Kang, C. Y., J. Tang, L. M. Li, H. B. Pan, P. S. Xu, S. Q. Wei, et al. In situ study on the electronic structure of graphene grown on 6H–SiC (0 0 0 $\bar{1}$) with synchrotron radiation photoelectron spectroscopy. *Applied Surface Science*, Vol. 258, 2012, pp. 2187–2191.

[27] Ren, H., B. W. Li, X. Y. Zhou, S. Chen, Y. M. Li, C. L. Hu, et al. Wafer-size VO_2 film prepared by water-vapor oxidant. *Applied Surface Science*, Vol. 525, 2020, id. 146642.

[28] Sunmin, R., L. Liu, B. Stephane, Y. J. Yu, H. T. Liu, P. Kim, et al. Atmospheric oxygen binding and hole doping in deformed graphene on a SiO_2 substrate. *Nano Letters*, Vol. 10, 2010, pp. 4944–4951.

[29] Briggs, N., B. Bersch, Y. X. Wang, J. Jiang, R. J. Koch, N. Nayir, et al. Atomically thin half-van der Waals metals enabled by confinement heteroepitaxy. *Nature Materials*, Vol. 19, 2020, pp. 637–643.

[30] Faugeras, C., A. Nerrière, M. Potemski, A. Mahmood, E. Dujardin, C. Berger, et al. Few-layer graphene on SiC, pyrolitic graphite, and graphene: A Raman scattering study. *Applied Physics Letters*, Vol. 92, 2008, id. 011914.

[31] Kang, C. Y., L. L. Fan, S. Chen, Z. L. Liu, P. S. Xu, and C. W. Zou. Few-layer graphene growth on 6H-SiC (0001) surface at low temperature via Ni-silicidation reactions. *Applied Physics Letters*, Vol. 100, 2012, id. 251604.

[32] Kazuma, Y., T. Takayuki, K. Atsushi, and T. Kazutoshi. Fabrication of a single layer graphene by copper intercalation on a SiC (0001) surface. *Applied Physics Letters*, Vol. 104, 2014, id. 053115.

[33] Wang, Z. J., A. Y. Dong, M. M. Wei, Q. Fu, and X. H. Bao. Graphene as a surfactant for metal growth on solid surfaces: Fe on graphene/SiC (0001). *Applied Physics Letters*, Vol. 104, 2014, id. 181604.

[34] Lee, D. and J. Seo. Graphene growth on sapphire via palladium silicidation. *Applied Surface Science*, Vol. 492, 2019, pp. 23–26.

[35] Weatherup, R. S., B. C. Bayer, and B. Raoul. In situ characterization of alloy catalysts for low-temperature graphene growth. *Nano Letters*, Vol. 11, 2011, pp. 4154–4160.

[36] Kim, H. W., I. Song, and T. H. Kim. Millimeter-scale growth of single-oriented graphene on a palladium silicide amorphous film. *ACS Nano*, Vol. 13, 2019, pp. 1127–1135.

[37] Jiang, M., X. Cao, S. H. Bao, H. J. Zhou, and P. Jin. Regulation of the phase transition temperature of VO_2 thin films deposited by reactive magnetron sputtering without doping. *Thin Solid Films*, Vol. 562, 2014, pp. 314–318.

[38] Cheng, X. K., Q. Gao, K. F. Li, Z. L. Liu, Y. X. Zhang, B. Li, et al. Enhanced phase transition properties of VO_2 thin films on 6H-SiC (0001) substrate prepared by pulsed laser deposition. *Nanomaterials*, Vol. 9, 2019, id. 1061.

[39] Ren, G. F., R. B. Zhang, and Z. Y. Fan. VO_2 nanoparticles on edge oriented graphene foam for high rate lithium ion batteries and supercapacitors. *Applied Surface Science*, Vol. 441, 2018, pp. 466–473.

[40] Zhang, S. X., J. Y. Chou, and L. J. Lauhon. Direct correlation of structural domain formation with the metal insulator transition in a VO_2 nanobeam. *Nano Letters*, Vol. 9, 2009, pp. 4527–4532.

[41] Kang, C. Y., C. Zhang, L. W. Zhang, S. S. Liang, C. C. Geng, G. H. Cao, et al. Transformation of crystalline structure and photoelectric properties in VO_2/glass thin films by inserting TiO_2 buffer layers. *Applied Surface Science*, Vol. 463, 2019, pp. 704–712.

[42] Liang, J. R., X. Yu, Y. R. Zhao, X. W. Fan, W. H. Wu, and S. L. Wang. Enhancement of metal-insulator transition performance of VO_2 thin films by conventional furnace annealing. *Thin Solid Films*, Vol. 730, 2021, id. 138709.

[43] Chen, S., Z. W. Wang, L. L. Fan, Y. L. Chen, H. Ren, H. Ji, et al. Sequential insulator-metal-insulator phase transitions of VO_2 triggered by hydrogen doping. *Physical Review B*, Vol. 96, 2017, id. 125130.

[44] Aetukuri, N. B., A. X. Gray, and D. Marc. Control of the metal–insulator transition in vanadium dioxide by modifying orbital occupancy. *Nature Physics*, Vol. 9, 2013, pp. 661–666.

[45] Fan, L. L., S. Chen, Z. L. Luo, Q. H. Liu, Y. F. Wu, L. Song, et al. Strain dynamics of ultrathin VO_2 film grown on TiO_2 (001) and the associated phase transition modulation. *Nano Letters*, Vol. 14, 2014, pp. 4036–4043.

[46] Bharathi, R. and A. M. Umarji. Phase evolution and infrared transmittance in monophasic VO_2 synthesized by a rapid non-equilibrium process. *Materials Chemistry and Physics*, Vol. 190, 2017, pp. 219–229.

[47] Bharathi, R., N. Rameshwari, and A. M. Umarji. Metal–insulator transition characteristics of vanadium dioxide thin films synthesized by ultrasonic nebulized spray pyrolysis of an aqueous combustion mixture. *Journal of Physics D: Applied Physics*, Vol. 48, 2015, id. 305103.

[48] Yu, W. L., S. Li, and C. Huang. Phase evolution and crystal growth of VO_2 nanostructures under hydrothermal reactions. *RSC Advances*, Vol. 6, 2016, pp. 7113–7120.

[49] Lin, H. R., X. H. Guo, K. X. Song, J. Feng, S. L. Li, and X. F. Zhang. Synergistic strengthening mechanism of copper matrix composite reinforced with nano-Al_2O_3 particles and micro-SiC whiskers. *Nanotechnology Reviews*, Vol. 10, 2021, pp. 62–72.

[50] Dong, X. D., A. Q. Wang, J. P. Xie, and Z. Wang. Optimization of volume fraction and microstructure evolution during thermal deformation of nano-SiCp/Al–7Si composites. *Nanotechnology Reviews*, Vol. 10, 2021, id. 1.